

An Investigation of 2nd-Order Fixed Point SLIP Behavior

Ioannis Kontolatis, and Evangelos Papadopoulos, *Senior Member, IEEE*

Abstract— This paper introduces alternative behaviors described by the SLIP model when it is subject to a range of initial conditions. A non-dimensional SLIP model and a numerical return map search scheme are used to determine fixed points as a function of non-dimensional leg stiffness and vertical displacement under friction constraints. A SLIP model behavior analysis is performed, using an analytical stance phase approximation, by diverging from the fixed points, i.e. by increasing/decreasing initial horizontal velocity, and/or touchdown angle. The results show that beyond the regular fixed points, the SLIP model performs an alternative, stable behavior that repeats itself every two cycles of motion. We call these 2nd-order fixed points and the regular ones 1st-order fixed points. A numerical simulation scheme was developed to investigate 2nd-order fixed points for a wide range of horizontal velocities and touchdown angles. Results show that 2nd-order fixed points respecting the friction cone constraints exist that can lead to a number of different behaviors such as high jumps, obstacle avoidance of different heights, or backward motion.

I. INTRODUCTION

The Spring Loaded Inverted Pendulum (SLIP) template describes the dynamic behavior during locomotion of a number of animals, and is used for several robot design and control implementations [1]. To name a few, a monopod robot that exploits an underwater SLIP version (U-SLIP) is presented in [2]. An extended 3D Dual-SLIP walking strategy for uneven terrains was used to generate trajectories for a biped model [3]. To preserve a SLIP-like hip trajectory during low velocities, researchers add energy by actively compressing the leg spring of a compliant quadruped robot at mid-stance [4]. A new version of the hexapod SLIP-based runner, and a more detailed dynamic model (R2-SLIP) were presented [5]. These robots exploit the SLIP model to achieve a limit cycle forward motion using parameter values and initial conditions inside a “safe” range without considering alternative behaviors like high jumps, or moving backwards.

Following the introduction of the SLIP model, its behavior for different initial conditions and its limits were investigated. A J-shaped dependency was determined between the angle of attack and leg stiffness for periodic motion patterns at a running speed; conditions except forward running were not investigated [6]. Although further analysis led to expressions characterizing periodic gaits, and their stability and bifurcations [7], constraints like friction were not taken into consideration, and period-doubling behaviors were not investigated in detail. Stable cycles of higher periods appeared when a planar, passive, two-link model resembling a human leg was exploited [8] for initial conditions and stability estimates to be found.

The SLIP model is an ideal model that needs to be adjusted when used in real-world applications. A robotic leg is controlled to realize an undamped SLIP model by

cancelling the undesired damping factors through positive feedback based on Kalman filter estimates [9]. A hopping robot designed as a realization of the running SLIP model utilizes a linearized Raibert step controller to achieve extreme jumping and forwards-backwards locomotion with external position feedback [10]. Using the swing leg retraction (SLR) method, the otherwise unstable conservative SLIP model can be stabilized and controlled, and the non-conservative SLIP can have increased robustness [11]. An extension of the SLIP model by adding a hip actuation to compose a tail-actuated one (TSLIP) was presented in [12].

The SLIP model is a simple mass-spring system; however only an approximate analytical solution predicting the center of mass trajectory during the stance phase can be obtained. The “bottom-to-apex” return map approximations are calculated using the iterated application of the mean value theorem for integral operators applied to a nonintegrable system perturbation [13]. Stance phase equations of motion were simplified by assuming a small angular sweep and spring compression [14]. Results show that for spring compression up to 20%, angle of attack ≥ 60 deg. and angular sweep ≤ 60 deg., the approximation yields 1% spring compression and 0.6 deg. angular tolerance.

In this paper, we investigate alternative behaviors described by the SLIP model, when it is subject to a range of initial conditions. Non-dimensional equations of motion of the SLIP model and a numerical return map search scheme to are employed to determine fixed points as a function of non-dimensional leg stiffness and vertical displacement under friction constraints. We perform an analysis of the SLIP model behavior by diverging from the fixed points, i.e. by increasing/decreasing initial horizontal velocity and/or touchdown angle. For this analysis, we use an analytical approximation for the stance phase. The results show that beyond the determined fixed points, the SLIP model exhibits alternative, stable behaviors that repeat themselves every *two* cycles of motion. We call these 2nd-order fixed points, and the regular ones 1st-order for consistency. Due to limitations of the analytical approximation, a numerical simulation scheme is developed to investigate 2nd-order fixed points for a wider range of horizontal velocities and touchdown angles. Results show that 2nd-order fixed points observing the friction constraints do exist, and can lead to a number of different behaviors such as high jumps, obstacle avoidance of different heights, or backward motion. These fixed points exist in a continuous space, and transitions between them can be achieved at the next cycle of motion by simply changing the touchdown angle and/or the forward velocity.

II. SLIP MODEL

The SLIP model was introduced to describe dynamic legged locomotion in the simplest way. The model is planar, conservative, and consists of a point mass equal to a system’s total mass and a massless spring as the compliant leg (Fig. 1).

The authors are with the School of Mechanical Engineering, National Technical University of Athens, (e-mail: egpapado@central.ntua.gr, tel: +30 210-772-1440).

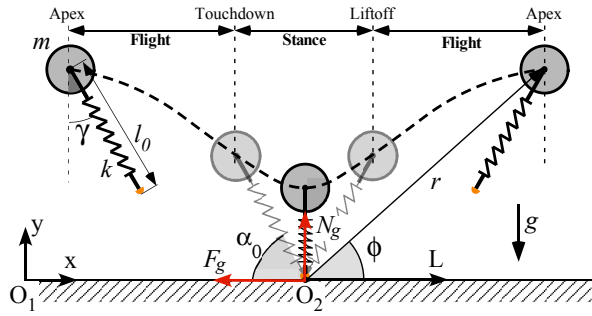


Figure 1. The SLIP model, basic variables, and its two phases.

A. Phase dynamics

The SLIP model has two phases, *flight* and *stance*. For the stance phase, the SLIP leg-ground interaction model assumes a rigid terrain, and a revolute joint connecting leg and terrain. For this assumption to hold, the leg should not slip, i.e. the reaction force must be in the friction cone defined by

$$F_G \leq (\text{CoF})N_G \quad (1)$$

where CoF is the coefficient of friction, F_G is the ground horizontal force, and N_G is the vertical ground force, see Fig. 1. In addition, N_G should not be negative. Both reaction force components are obtained using a Newton-Euler formulation,

$$F_G = m\ddot{x} - k(l_0 - l)\sin\gamma \quad (2)$$

$$N_G = m(\ddot{y} + g) + k(l_0 - l)\cos\gamma \quad (3)$$

Using Cartesian coordinates and a Lagrangian formulation, the equations of motion for the stance phase are

$$\ddot{\mathbf{x}} = \begin{bmatrix} \ddot{x} \\ \ddot{y} \end{bmatrix} = - \begin{bmatrix} 1/m & 0 \\ 0 & 1/m \end{bmatrix} \begin{bmatrix} k(x_{td} - x)L \\ mg - kyL \end{bmatrix} \quad (4)$$

where all variables are defined in Table I, and

$$L = \left(l_0 - \left[(x_{td} - x)^2 + y^2 \right]^{1/2} \right) \left[(x_{td} - x)^2 + y^2 \right]^{-1/2} \quad (5)$$

while the rest of variables and parameters are presented in Table I. Flight phase equations of motion are derived using (4) by zeroing the compliance terms. A more compact form can be derived, if the following

$$l = \left[(x_{td} - x)^2 + y^2 \right]^{1/2} \quad (6)$$

$$\sin(\gamma) = (x_{td} - x) \left[(x_{td} - x)^2 + y^2 \right]^{-1/2} \quad (7)$$

$$\cos(\gamma) = y \left[(x_{td} - x)^2 + y^2 \right]^{-1/2} \quad (8)$$

are substituted in (4):

$$\begin{bmatrix} \ddot{x} \\ \ddot{y} \end{bmatrix} = \begin{bmatrix} -(k/m)(l_0 - l)\sin(\gamma) \\ -g + (k/m)(l_0 - l)\cos(\gamma) \end{bmatrix} \quad (9)$$

B. Threshold functions

The flight phase ends with a touchdown and the flight starts with a leg liftoff, see Fig. 1. These events are triggered according to the zero crossings of the threshold functions:

$$h_{1,2} = y - l_0 \cos(\gamma_{td}) \quad (10)$$

$$h_{2,1} = l - l_0 \quad (11)$$

When (10) is zero crossed, the Center of Mass (CoM) y-axis coordinate allows the leg tip (toe) to just touch the ground for a given touchdown angle γ_{td} corresponding to the transition

from *flight* to *stance*. When (11) is zero crossed, the spring length is equal to the uncompressed value and corresponds to the transition from *stance* to *flight* phase. Each threshold function is used only when then appropriate phase is in progress, i.e. (10) for the flight and (11) for the stance phase.

TABLE I. SLIP PARAMETERS AND VARIABLES.

Symbol	Quantity
x (m)	Body CoM x-axis coordinate w.r.t. $\mathbf{O}_1\mathbf{x}\mathbf{y}$
y (m)	Body CoM y-axis coordinate w.r.t. $\mathbf{O}_1\mathbf{x}\mathbf{y}$
m (kg)	Body mass
l (m)	Spring length
l_0 (m)	Spring uncompressed length
k (N/m)	Spring constant
γ (deg)	Spring angle w.r.t. $\mathbf{O}_1\mathbf{x}\mathbf{y}$
g (m/s ²)	Gravity acceleration
r (m)	Body CoM radial coordinate w.r.t. $\mathbf{O}_2\mathbf{L}$
ϕ (deg)	Body CoM angular coordinate w.r.t. $\mathbf{O}_2\mathbf{L}$
a_0	Angle of attack
td	As index: value at touchdown
lo	As index: value at liftoff
0	As index: variable initial values
1	As index: flight phase
2	As index: stance phase
*	As exponent: nondimensionalised parameter/variable

C. Dimensional Analysis

Despite its simplicity, the SLIP model holds complicated relations between parameters and variables, mostly due to coupling. To investigate these relations, and to obtain results and conclusions for different designs, non-dimensionalization is employed. The non-dimensional variable of time t is:

$$t^* = t / s \quad (12)$$

where s is a time scale chosen to be the pendulum period, as this is usually slower than spring oscillation:

$$s = (l_0 / g)^{1/2} \quad (13)$$

All lengths are non-dimensionalized using the spring uncompressed length l_0 :

$$\mathbf{x}^* = (1 / l_0)\mathbf{x}, \quad \dot{\mathbf{x}}^* = (s / l_0)\dot{\mathbf{x}}, \quad \ddot{\mathbf{x}}^* = (s^2 / l_0)\ddot{\mathbf{x}} \quad (14)$$

$$l^* = l / l_0 \quad (15)$$

while the spring angle and its derivatives become,

$$\gamma^* = \gamma, \quad \dot{\gamma}^* = s\dot{\gamma}, \quad \ddot{\gamma}^* = s^2\ddot{\gamma} \quad (16)$$

Using (14)-(16), the stance phase equations of motion (9) take the non-dimensionalized form:

$$\begin{bmatrix} \ddot{x}^* \\ \ddot{y}^* \end{bmatrix} = \begin{bmatrix} -(k/m)s^2(1-l^*)\sin(\gamma^*) \\ -(s^2/l_0)g + (k/m)s^2(1-l^*)\cos(\gamma^*) \end{bmatrix} \quad (17)$$

where l^* and γ^* are given from:

$$l^* = \left[(x_{td}^* - x^*)^2 + y^{*2} \right]^{1/2} \quad (18)$$

$$\gamma^* = \text{atan}(y^*, x_{td}^* - x^*) \quad (19)$$

If the time scale s is substituted using (13) and the relative leg stiffness R defined as:

$$R = (kl_0) / (mg) \quad (20)$$

is used, (17) takes a simpler form:

$$\begin{bmatrix} \ddot{x}^* \\ \ddot{y}^* \end{bmatrix} = \begin{bmatrix} -R(1-l^*)\sin(\gamma^*) \\ -1 + R(1-l^*)\cos(\gamma^*) \end{bmatrix} \quad (21)$$

Threshold functions (10) and (11) change likewise:

$$h_{1,2}^* = y^* - \cos(\gamma_{td}^*) \quad (22)$$

$$h_{2,1}^* = l^* - 1 \quad (23)$$

III. FIXED POINT SEARCH SCHEME

A fixed point search scheme, similar to the one used in [15], has been developed using MATLAB and applied to the non-dimensionalized SLIP model (21) - (23) to determine which initial conditions at apex, i.e. touchdown angle $\gamma_{td,0}$ and horizontal velocity \dot{x}_0^* , yield steady state cyclic motions for a given initial vertical displacement y_0^* .

The return map \mathbf{P} is defined using the apex height of the motion cycle, i.e. the maximum vertical displacement. A function is needed that maps the apex height states of the initial cycle n to those of the next one ($n+1$). If the state vector at the next cycle is equal to the initial, then the cycle is repeatable, i.e. a fixed point is identified. The initial touchdown angle $\gamma_{td,0}$ and the initial horizontal velocity \dot{x}_0^* at apex are considered as the search space states $\boldsymbol{\chi}$, while the initial vertical displacement y_0^* at apex is the input parameter u which is kept constant during the search. The system of equations whose solution is sought is of the form,

$$\boldsymbol{\chi}_{n+1} = \mathbf{P}(\boldsymbol{\chi}_n, u_n) \quad (24)$$

$$\boldsymbol{\chi} = [\dot{x}_0^* \quad \gamma_{td,0}]^T \quad \text{and} \quad u = y_0^* \quad (25)$$

In the analysis presented in this paper y_0^* was chosen to have value equal to 1.273 to meet a specific vertical displacement-leg length ratio which corresponds to a medium sized legged robot. Likewise, the relative leg stiffness R value is in the range of 40 to 140. The analysis can be extended to different range values of y_0^* and R . The initial touchdown angle $\gamma_{td,0}$ and horizontal velocity \dot{x}_0^* ranges have been chosen to exceed realistic values so that the results provide general conclusions and patterns. The identified fixed points form a continuous surface, see Fig. 2, and show that the touchdown angle $\gamma_{td,0}$ increases as relative leg stiffness R decreases and/or horizontal velocity \dot{x}_0^* increases.

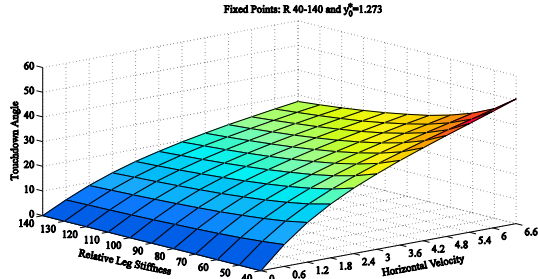


Figure 2. Fixed points for R 40-140 and initial vertical displacement 1.273.

To determine fixed points for specific SLIP parameters set, i.e. $m=4\text{kg}$, $k=12000\text{N/m}$ and $l_0=0.275\text{m}$, and initial conditions, i.e. $x_0=0\text{m}$, $y_0=0.35\text{m}$ and $\dot{y}_0=0\text{m/s}$, first the non-dimensionalized variables and parameter are computed as: $R=84.1$, $x_0^*=0$, $y_0^*=1.273$, $\dot{y}_0^*=0$. The results for the specific values form a continuous line and are presented in Fig. 3. The CoF was chosen to be 0.7 as the mean value for concrete – rubber interactions. The large circle marker (blue) fixed points satisfy the friction cone constraints, while the small full circle (red) ones do not and the motion is not achievable for the given CoF. Note that the friction cone constraints are implemented after the fixed point detection. If the CoF is

increased, more small full circle fixed points will become large, but of course their value will not change.

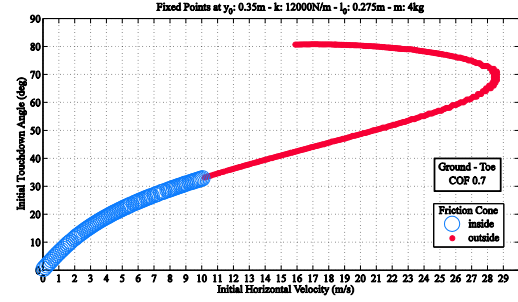


Figure 3. Fixed points using friction cone constraints with 0.7 COF.

IV. FIXED POINT ANALYSIS

Fixed points found in Sect. III using the apex return map satisfy the property for periodic motion. If the passive and conservative SLIP model is released with an initial energy level at apex, i.e. initial vertical displacement y_0 , horizontal velocity \dot{x}_0 and vertical velocity $\dot{y}_0=0$, and the initial touchdown angle $\gamma_{td,0}$ (energy allocation) which corresponds to the given horizontal velocity (fixed point) is used, then the response is an infinitely repeatable motion with the same characteristics in all cycles. *But what happens if the initial energy level (\dot{x}_0) and/or energy allocation ($\gamma_{td,0}$) are different from the ones calculated as the fixed point values? And what happens as the values diverge from the ones of Fig. 2?*

To answer these questions, the analytical approximation for the center of mass trajectory during stance phase described in [14] was exploited. This approximation is valid for spring compressions up to 20%, angle of attack $\geq 60\text{deg}$. and angular sweep $\leq 60\text{deg}$. [14]. The analytical solution during the flight phase is a ballistic trajectory. The polar coordinates (r, φ) (Fig. 1) are used to describe the SLIP motion during stance phase. The trajectory is given by

$$r(t) = l_0 - \frac{|\dot{r}_{td}|}{\hat{\omega}_0} \sin \hat{\omega}_0 t + \frac{\hat{\varphi}_{td}^2 l_0 - g}{\hat{\omega}_0^2} (1 - \cos \hat{\omega}_0 t) \quad (26)$$

$$\varphi(t) = \pi - \alpha_0 + \left(1 - 2(\hat{\varphi}_{td}^2 - g/l_0)\hat{\omega}_0^{-2}\right)\hat{\varphi}_{td} t + 2\hat{\varphi}_{td}\hat{\omega}_0^{-1} \left[(\hat{\varphi}_{td}^2 - g/l_0)\hat{\omega}_0^{-2} \sin \hat{\omega}_0 t + |\dot{r}_{td}|(\hat{\omega}_0 l_0)^{-1} (1 - \cos \hat{\omega}_0 t) \right] \quad (27)$$

where

$$\hat{\omega}_0 = \left[k/m + 3(r_{td}^2 \hat{\varphi}_{td} l_0^{-2}) \right]^{1/2} \quad (28)$$

Polar coordinates (r_{td}, φ_{td}) and speeds at touchdown are calculated using the flight phase ballistic trajectory analytical equations. The stance phase duration is:

$$t_{st} = \left[\pi + 2 \arctan \left((g - l_0 \hat{\varphi}_{td}^2) / (|\dot{r}_{td}| \hat{\omega}_0) \right) \right] / \hat{\omega}_0 \quad (29)$$

The fixed point analysis scheme initiates from a fixed point at apex $(\gamma_{td,0}, y_0, \dot{x}_0, \dot{y}_0=0\text{m/s})$ and uses the flight phase analytical equations to calculate the CoM trajectory for the phase duration (t_{fl}) . Then the analytical approximation for the stance phase trajectory (26)-(28) is used for the appropriate duration (t_{st}) calculated using (29) with touchdown values the flight phase last ones. The process repeats itself with liftoff values for the flight phase, the stance phase last values. Each motion cycle is considered from apex to apex.

At first, the fixed point at $\dot{x}_0=1.0\text{m/s}$ and $\gamma_{td,0}=6.13\text{deg}$. was chosen for the analysis as it fulfills the approximation constraints for small angular sweep and spring compression.

The results of the analytical calculations are presented in Table II under the column “Fixed Point”.

	Variable	Fixed Point	Point 1	Point 2
START CYCLE 1				
Apex1	\dot{x}_0 (m/s)	1.000	1.500	1.000
	y_0 (m)	0.350	0.350	0.350
	$\gamma_{td,0}$ (deg)	6.13	6.13	12.00
	t_{fl} (s)	0.125	0.125	0.129
	y_{td} (m)	0.273	0.273	0.269
TD1	$\dot{\phi}_{td}$ (rad/s)	-3.140	-4.948	-2.604
	t_{st} (s)	0.060	0.058	0.061
END CYCLE 1 – START CYCLE 2				
Apex2	\dot{x} (m/s)	0.999	1.652	0.580
	y (m)	0.350	0.326	0.384
	γ_{td} (deg)	6.11	12.31	-1.73
	t_{fl} (s)	0.125	0.108	0.149
	y_{td} (m)	0.273	0.269	0.275
TD2	$\dot{\phi}_{td}$ (rad/s)	-3.138	-5.049	-2.269
	t_{st} (s)	0.060	0.058	0.061
END CYCLE 2 – START CYCLE 3				
Apex3	\dot{x} (m/s)	0.999	1.505	0.993
	y (m)	0.350	0.349	0.357
	γ_{td} (deg)	6.11	6.41	11.95
	t_{fl} (s)	0.125	0.124	0.130
	y_{td} (m)	0.273	0.273	0.270

The response can be seen in Figs. 4 and 5 (blue line) and is periodic. Every variable value at the end of every cycle is equal to the initial value and every cycle is identical, as expected. Consequently, the initial horizontal velocity value \dot{x}_0 is increased from fixed point value while the rest variables, i.e. $\gamma_{td,0}$, y_0 , \dot{y}_0 , are kept the same. The new response differs from the fixed point one and is presented in Fig. 4. The results of the analytical calculations are presented in Table II under the column “Point 1”. At the end of the first cycle, values are not equal to the initial ones, more specifically the CoM vertical displacement y is reduced and the horizontal velocity \dot{x} is increased. At the end of the second cycle though, both variables return to their initial values. This behavior is repeatable every two cycles. The response is never attracted to that of the corresponding fixed point nor does it become unstable. The two responses have a phase offset due to the horizontal velocity increment. Similar behavior is observed when instead of the horizontal velocity, the initial touchdown angle is increased.

In this case, at the end of the first cycle the vertical displacement is increased and the horizontal velocity is reduced. The results of the analytical calculations are presented in Table II under the column “Point 2”. Again, this behavior repeats every two cycles as it can be seen in Fig. 5.

Also, Fig. 5 shows clearly that the initial touchdown angle acts as an energy “allocator”, since both sets of initial conditions, i.e. fixed point and increased touchdown angle, have the same energy level (\dot{x}_0 , y_0 , \dot{y}_0). In this way, the maximum vertical displacement (apex height) can be altered by changing only the touchdown angle of every cycle. This result is in complete agreement with Raibert’s initial findings [16]. In the case of Fig. 4, the maximum vertical displacement can be altered also, but to obtain this behavior energy needs to be pumped (or dumped) into the system to increase (or decrease) its initial level as the touchdown angle is the same at every cycle. As the SLIP model is passive and

conservative, the initial total energy level does not change but is distributed differently between the potential and kinetic.

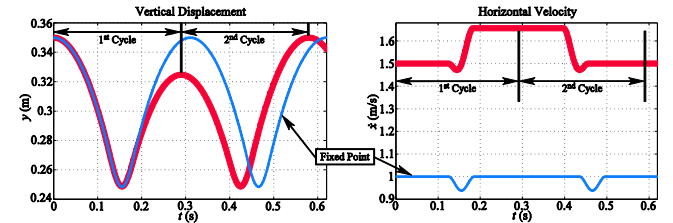


Figure 4. SLIP response at $\dot{x}_0=1.5\text{m/s}$, $y_0=0.35\text{m}$, $\gamma_{td,0}=6.13\text{deg}$. (thick red line) and at fixed point $\dot{x}_0=1.0\text{m/s}$, $y_0=0.35\text{m}$, $\gamma_{td,0}=6.13\text{deg}$. (thin blue line).

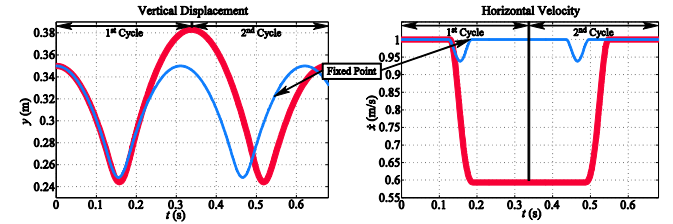


Figure 5. SLIP response at $\dot{x}_0=1.0\text{m/s}$, $y_0=0.35\text{m}$, $\gamma_{td,0}=12\text{deg}$. (thick red line) and at fixed point $\dot{x}_0=1.0\text{m/s}$, $y_0=0.35\text{m}$, $\gamma_{td,0}=6.13\text{deg}$. (thin blue line).

Using the fixed point analysis scheme described in this paragraph, we specified that if the initial values vary from those of the fixed point, then the SLIP model exhibits again an infinitely periodic motion, but with different characteristics and without becoming unstable or attracted towards some other behavior. The difference of this motion compared to that of the fixed point increases as the initial values diverge from it. Therefore, although we replied the question posed at the start of Sect. IV, a new question reasonably arises. *Are there any boundaries for this kind of behavior, and what happens for extreme values of horizontal velocity and touchdown angle?* To answer this question, a numerical scheme is developed to extend the range limitation of the stance phase approximate analytical solution.

V. FIXED POINT BEHAVIOR

To evaluate the fixed points, a numerical scheme has been programmed in MATLAB. The simulation core is the SLIP equations of motion. Each set of phase equations is integrated using the ODE45 function for the current time until the time the next phase threshold function triggers.

The response that corresponds to the fixed points in Fig. 2 is, as expected, the same and infinitely repeatable per cycle, see Fig. 6. When initial conditions differ from fixed point values, a repeatable behavior occurs, but with an-every-second-cycle pattern. For consistency, we call these points “2nd-order fixed points”, while the single cycle fixed points (Figs. 2 & 3), “1st-order fixed points.”

Using the fixed point evaluation numerical scheme, plot areas and boundary lines were determined and are shown in Fig. 7. These areas and their boundaries describe different behaviors of the SLIP model according to the initial energy level, i.e. initial horizontal velocity \dot{x}_0 and vertical displacement y_0 , and energy allocation, i.e. initial touchdown angle $\gamma_{td,0}$. The blue line corresponds to the 1st-order fixed points, see Fig. 6. Areas 1 to 3 are defined by the boundary lines depicted with different colors in Fig. 7. The two black lines set the limit for leg stumbling. The leg stumbles because at the end of the first cycle, the apex height does not allow for

adequate leg clearance for the specific touchdown angle. It is worth noting that the two black line limits exist because in both Areas 1 and 3, the vertical displacement at the end of the first cycle is lower than the initial one, and keeps lowering as we move towards the black lines until intersection.

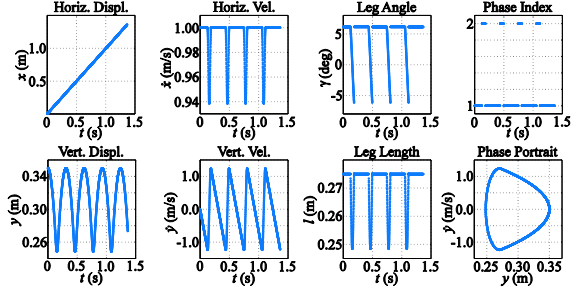


Figure 6. 1st-order fixed point at $\dot{x}_0=1\text{m/s}$ $y_0=0.35\text{m}$ $\gamma_{td,0}=6.13$ deg.

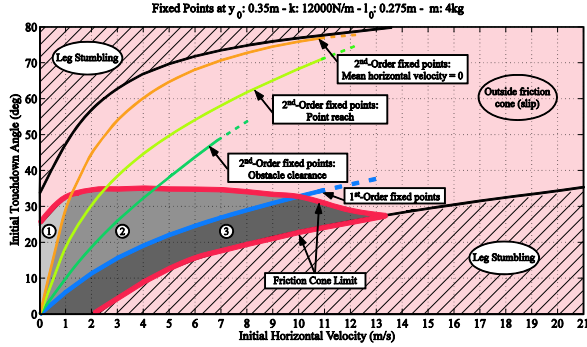


Figure 7. SLIP model fixed points: areas and boundaries.

The red line sets the friction cone limit, beyond of which the leg slips. For the current analysis, the CoF between the ground and the leg toe was chosen to be 0.7 (as in Sect. III). If the CoF for example takes a higher value, the red line will extend to greater touchdown angles and horizontal velocities.

The orange line sets the boundary between Areas 1 and 2 and is the limit at which the horizontal velocity at the end of the first cycle is equal and opposite to the initial one, resulting to zero mean horizontal displacement with the SLIP model oscillating between two opposite horizontal positions ($-x, x$).

Two more lines exist within Area 2 which are not boundaries but point to useful properties. The dark green line or *obstacle clearance line* indicates 2nd-order fixed points that at the end of first cycle have a maximum vertical displacement (*Height1*) determined by a horizontal velocity (*HozVel1*) which is maximum for this vertical displacement. In other words, as we diverge from the dark green line, the vertical displacement or horizontal velocity or both at the end of the first cycle have lower values compared to the ones on the line. The light green line or *point reach line* indicates 2nd-order fixed points that at the end of the first cycle have the maximum vertical displacement (*Height2*) and horizontal velocity of zero value (*HozVel2*). The points of this line indicate the touchdown angle that allocates all the energy to vertical displacement for a given initial horizontal velocity. It should be noted here that maximum performance in terms of velocity or apex height depends on the initial energy level, i.e. on the horizontal velocity and vertical displacement.

For a lower initial touchdown angle and/or greater initial horizontal velocity than those on the blue line, i.e. plot Area 3, the SLIP model results in the response of Fig. 8. At the end

of the first cycle (second cycle initial conditions), the vertical displacement y is lower and the horizontal velocity \dot{x} is larger than those of the initial conditions. At the end of the second cycle, the y and \dot{x} values are equal to the initial ones. Note that for a 1st-order fixed point (blue line), y and \dot{x} are equal to their initial values at the end of first and each other cycle.

For a higher initial touchdown angle and/or lower initial horizontal velocity from the blue line, i.e. Area 2, the SLIP model results in the response of Fig. 9. At the end of the first motion cycle, y is greater and \dot{x} is lower than the initial ones, while at the end of the *second* cycle the values are equal to the initial ones. The SLIP response for Area 1 in Fig. 7 is shown in Fig. 10. At the end of the first cycle, y is smaller than the initial value as in the case of points in Area 3, Fig. 7.

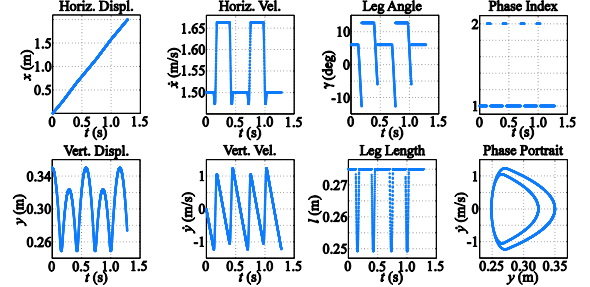


Figure 8. Area 3 2nd-order fixed point at $\dot{x}_0=1.5\text{m/s}$ $y_0=0.35\text{m}$ $\gamma_{td,0}=6.13$ deg.

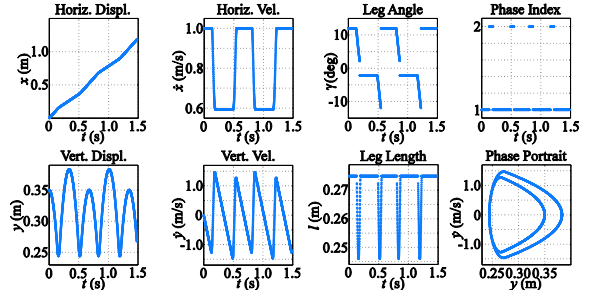


Figure 9. Area 2 2nd-order fixed point at $\dot{x}_0=1\text{m/s}$ $y_0=0.35\text{m}$ $\gamma_{td,0}=12$ deg.

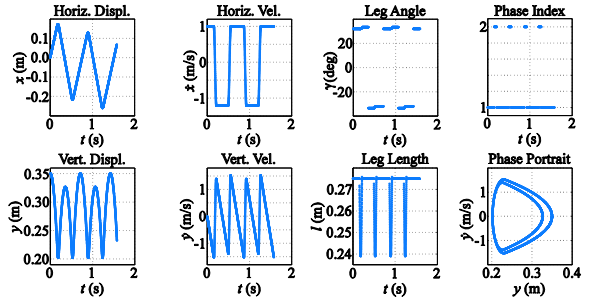


Figure 10. Area 1 2nd-order fixed point at $\dot{x}_0=1\text{m/s}$ $y_0=0.35\text{m}$ $\gamma_{td,0}=32$ deg.

The horizontal velocity, on the other hand, is negative and its absolute value is larger than the initial one. In this area, the SLIP overall horizontal displacement is in the opposite direction from the initial horizontal velocity, i.e. the system moves backwards. The difference response magnitude between 1st-order and 2nd-order fixed points depends on the difference magnitude between their initial values. The more different the I.C.'s are, the more different the response is.

VI. DISCUSSION

The SLIP response when initial conditions are perturbed was studied first using an analytical approximation for the stance phase dynamics. Results demonstrated that even if the initial

conditions diverge, again an infinitely repeatable behavior is achieved which comes back to the initial conditions at the end of every *second cycle* (2nd-order fixed points). These results are in agreement with the ones in [8] and [9]. Using them as a starting point and due to the approximation limitations associated with angular sweep and spring compression, a numerical search scheme was developed next, which investigated the full range of robot parameters and initial conditions under friction constraints. Results showed that within the friction constraint area in Fig. 7, distinct sub-areas with specific characteristics and useful properties exist, beyond the set and line of the 1st-order fixed points.

The 2nd-order fixed points of Areas 2 and 3 exhibit similar behavior. At the end of the first cycle, SLIP in Area 2 performs a motion of higher vertical displacement and lower horizontal velocity than the initial conditions; vice versa in Area 3. These areas show that the SLIP model motion characteristics for a given robot parameter set can be altered by changing the energy level, i.e. the horizontal velocity, or the energy allocation, i.e. the touchdown angle, while stability and repeatability are maintained. In Area 1, the 2nd-order fixed points lead to a negative horizontal velocity with greater absolute value than the initial one. A robot that exploits a fixed point of this area can change its motion direction and move backwards during the next cycle.

The *obstacle clearance* line consists of 2nd-order fixed points that have a maximum vertical displacement (*Height1*) determined by a horizontal velocity (*HozVel1*) which is maximum for this vertical displacement. When the conditions of this line are met, a robot can surpass an obstacle of certain height with a maximum horizontal velocity. For the same energy level, higher obstacles can be surpassed, but with lower velocity, and vice versa. The *point reach* line is the upper limit of this behavior, as the 2nd-order fixed points of this line have the maximum vertical displacement (*Height2*) and horizontal velocity of zero value (*HozVel2*). A robot using the conditions of this line can perform during the next motion cycle a vertical *high jump* and reach a height related to its energy level and land at the same point. The *zero mean horizontal velocity* line consists of 2nd-order fixed points, whose horizontal velocities at the end of each cycle are opposite, resulting in zero mean horizontal velocity. A robot which is exploiting these conditions can oscillate between two points covering a certain ground displacement and reaching a certain height at the middle of its trajectory.

The 2nd-order fixed points of Areas 1-3 form a continuous space, and transition between them can be performed within one motion cycle. The energy level can be maintained constant or energy can be pumped or dumped. If the energy level is maintained constant, then fixed point transition can be achieved using the energy allocation variable, i.e. the touchdown angle. Otherwise, energy pumping or dumping can be used for transition, while the touchdown angle is kept constant. Certainly, a faster transition can be achieved when both the energy level and the allocation are altered.

VII. CONCLUSION

In this paper, we investigated alternative behaviors that are described by the SLIP model when it is subjected to a range of initial conditions. The non-dimensionalized equations of motion of the SLIP model were derived and used. A numerical return map search scheme was developed to

determine fixed points as a function of non-dimensional leg stiffness and vertical displacement under friction cone constraints. We performed an analysis of the SLIP model behavior by diverging from the fixed points, i.e. by increasing/ decreasing initial horizontal velocity and/ or touchdown angle. This analysis was conducted for variables and parameters corresponding to group of medium sized legged robots and an analytical approximation for the stance phase was exploited. The results showed that beyond the determined fixed points, the SLIP model shows an alternative, stable behavior that repeats itself every two cycles of motion. These were called 2nd-order fixed points, while the regular ones 1st-order. Due to limitations of the analytical approximation, a numerical simulation scheme was developed to extend the 2nd-order fixed point analytical investigation to a wider range of horizontal velocities and touchdown angles. Results showed that 2nd-order fixed points exist observing the friction cone constraints, and can lead to a number of different behaviors such as high jumps, obstacle avoidance of different heights, or backwards motion.

REFERENCES

- [1] R. Blickhan et al., "Similarity in multilegged locomotion: Bouncing like a monopode," *J. Comp. Phys. A*, v. 173, n. 5, 1993, pp. 509-517.
- [2] M. Calisti et al., "Hopping on uneven terrains with an underwater one-legged robot," *Proc. IEEE International Conference on Robotics and Automation (ICRA '16)*, Stockholm, Sweden, May 16-21, 2016.
- [3] Y. Liu et al., "Trajectory Generation for Dynamic Walking in a Humanoid over Uneven Terrain Using a 3D-Actuated Dual-SLIP Model," *Proc. IEEE International Conference on Intelligent Robots and Systems (IROS '15)*, Hamburg, Germany, Sept. 28 – Oct. 2, 2015.
- [4] A. Spröwitz et al., "Towards dynamic trot gait locomotion: Design, control, and experiments with Cheetah-cub, a compliant quadruped robot," *Int. J. Robotics Research*, Vol. 32, No. 8, 2013, pp. 932-950.
- [5] K. Huang et al., "Design and Performance Evaluation of a Bio-Inspired and Single-Motor-Driven Hexapod Robot with Dynamical Gaits," *Journal of Mechanisms and Robotics*, Vol. 7, No. 3, 2015.
- [6] A. Seyfarth et al., "A movement criterion for running," *Journal of Biomechanics*, Vol. 35, No. 5, 2002, pp. 649-655.
- [7] R. Ghigliazza et al., "A Simply Stabilized Running Model," *Journal of Applied Dynamical Systems*, Vol. 2, No. 2, 2003, pp. 187-218.
- [8] M. Garcia et al., "The Simplest Walking Model: Stability, Complexity, and Scaling," *Journal of Biomechanical Engineering*, Vol. 120, No. 2, 1998, pp. 281-288.
- [9] J. Cho et al., "Realizing Natural Springy Motion of a Robotic Leg by Cancelling the Undesired Damping Factors," *Proc. IEEE International Conference on Robotics and Automation (ICRA '17)*, Singapore, May 29 – June 3, 2017.
- [10] D. W. Haldane et al., "Repetitive extreme-acceleration (14-g) spatial jumping with Salto-1P," *Proc. IEEE International Conference on Intelligent Robots and Systems (IROS '17)*, Vancouver, BC, Canada, September 24 – 28, 2017.
- [11] O. Nir et al., "Swing Leg Retraction Using Virtual Apex Method for the ParkourBot Climbing Robot," *Proc. IEEE International Conference on Intelligent Robots and Systems (IROS '17)*, Vancouver, BC, Canada, September 24 – 28, 2017.
- [12] H. Yu et al., "Planar Hopping Control Strategy for Tail-Actuated SLIP Model Traversing Varied Terrains," *Proc. IEEE International Conference on Intelligent Robots and Systems (IROS '17)*, Vancouver, BC, Canada, September 24 – 28, 2017.
- [13] W. J. Schwind et al., "Approximating the Stance Map of a 2-DOF Monoped Runner," *J. Nonlin. Science*, v.10, n.5, 2000, pp. 533-568.
- [14] H. Geyer et al., "Spring-mass running: simple approximate solution and application to gait stability," *Journal of Theoretical Biology*, Vol. 232, No. 3, 2005, pp. 315-328.
- [15] I. Poulakakis et al., "On the stability of the Passive Dynamics of Quadrupedal Running with a Bounding Gate," *International Journal of Robotic Research*, Vol. 25, No. 7, 2006, pp. 669-688.
- [16] M. H. Raibert, *Legged Robots That Balance*. Cambridge, Mass.: MIT Press, 1986.